

# Cross-modal Causal Intervention for Alzheimer's Disease Prediction

Yutao Jin  
jinyutao@my.swjtu.edu.cn  
Southwest Jiaotong University  
Chengdu Shi, China

Haowen xiao  
xhaowen@my.swjtu.edu.cn  
Southwest Jiaotong University  
Chengdu Shi, China

Jielei Chu\*  
jieleichu@swjtu.edu.cn  
Southwest Jiaotong University  
Chengdu Shi, China

Fengmao Lv  
fengmaolv@swjtu.edu.cn  
Southwest Jiaotong University  
Chengdu Shi, China

Yuxiao Li  
wchyuxiaoli@outlook.com  
Sichuan University  
Chengdu Shi, China

Tianrui Li  
trli@swjtu.edu.cn  
Southwest Jiaotong University  
Chengdu Shi, China

## Abstract

Mild Cognitive Impairment (MCI) serves as a prodromal stage of Alzheimer's Disease (AD), where early identification and intervention can effectively slow the progression to dementia. However, diagnosing AD remains a significant challenge in neurology due to the confounders caused mainly by the selection bias of multi-modal data and the complex relationships between variables. To address these issues, we propose a novel visual-language causal intervention framework named Alzheimer's Disease Prediction with Cross-modal Causal Intervention (ADPC) for diagnostic assistance. Our ADPC employs large language model (LLM) to summarize clinical data under strict templates, maintaining structured text outputs even with incomplete or unevenly distributed datasets. The ADPC model utilizes Magnetic Resonance Imaging (MRI), functional MRI (fMRI) images and textual data generated by LLM to classify participants into Cognitively Normal (CN), MCI, and AD categories. Because of the presence of confounders, such as neuroimaging artifacts and age-related biomarkers, non-causal models are likely to capture spurious input-output correlations, generating less reliable results. Our framework implicitly eliminates confounders through causal intervention. Experimental results demonstrate the outstanding performance of our method in distinguishing CN/MCI/AD cases, achieving state-of-the-art (SOTA) metrics across most evaluation metrics. The study showcases the potential of integrating causal reasoning with multi-modal learning for neurological disease diagnosis.

## CCS Concepts

• Computing methodologies → Computer vision tasks.

## Keywords

Alzheimer's Disease, Causal Inference, Multi-modal Learning, Large Language Model

**Unpublished working draft. Not for distribution.**

Permission to make digital or hard copies of all or part of this work for personal or internal use, or the internal or personal use of specific clients, is granted by ACM for profit or commercial advantage and that copies bear this notice and the full citation on the first page. Copyrights for components of this work owned by others than the author(s) must be honored. Abstracting with credit is permitted. To copy otherwise, or republish, to post on servers or to redistribute to lists, requires prior specific permission and/or a fee. Request permissions from [permissions@acm.org](mailto:permissions@acm.org).

ACM MM, 2025, Dublin, Ireland

© 2018 Copyright held by the owner/author(s). Publication rights licensed to ACM.

ACM ISBN 978-x-xxxx-xxxx-x/YYYY/MM

<https://doi.org/XXXXXXX.XXXXXXX>

2025-07-21 01:01. Page 1 of 1–9.

## 1 Introduction

Alzheimer's Disease (AD) is an irreversible neurodegenerative disorder characterized by progressive cognitive decline and distinct neuropathological alterations in brain tissue. Its clinical manifestations follow a continuous progression from Mild Cognitive Impairment (MCI) to dementia stages: early-stage symptoms predominantly involve episodic memory decline, intermediate-stage symptoms include language dysfunction and executive ability impairment, and late-stage symptoms result in the loss of basic self-care capacity. Studies indicate that initiating treatment during the MCI phase can delay disease progression by 40%, making early diagnosis of AD a major focus for clinical research.

Clinical diagnostic methods can be summarised as a chained reasoning process based on medical test data and driven by medical knowledge. Specifically, the diagnostic process of AD usually relies on neuropsychological scales and brain imaging to provide support for the basic medical data, and further screening and gradual elimination of confounding factors, such as other disorders with different causes but similar manifestations, to arrive at a more accurate clinical diagnosis. Within this process, the exclusion of confounders is a central step in clinical diagnosis. If not Intervened upon, confounders distort the true causal effect, leading to biased estimates that deviate from the true causal relationship. In AD diagnosis, confounders may obscure genuine pathological signals, misrepresenting disease mechanisms. Confounders manifest in diverse forms. Lifestyle factors (e.g., smoking, exercise habits) or environmental exposures (e.g., air pollution) may simultaneously influence both AD risk and biomarker profiles (such as inflammatory cytokine levels), while biomarkers themselves serve as critical diagnostic criteria. Demographic imbalances in gender, race, or educational attainment within datasets can lead to delayed clinical manifestation of cognitive decline in populations with higher education levels. Additionally, artifacts in neuroimaging may be misclassified as AD-specific features, resulting in elevated false positive rates. The factors mentioned above pose a great challenge for early-stage clinical screening of AD and greatly affect the outcome of AD treatment.

In recent years, many studies have used deep learning approaches from the perspective of computer vision hoping to address early-stage AD diagnosis. For instance, due to the subtle structural changes in the brain of early-stage patients, traditional methods rely on manual pre-selection of lesion regions and fail to integrate multi-modal

clinical data (e.g., cognitive scores, genetic information), resulting in limited diagnostic accuracy. 3D-CNN[17] propose to automatically learn lesion regions through hierarchical 3D fully convolutional networks and incorporate multi-modal feature fusion to improve the sensitivity and specificity of early diagnosis.

To address the challenge of predicting MCI-to-AD progression hindered by data scarcity from hard-to-access MCI subtype labels (pMCI/sMCI), HOPE leverages widely available coarse-grained labels (NC/MCI/AD) and employs ordered learning to capture inherent disease progression patterns, thereby reducing reliance on subtype-specific annotations.

In addition, Due to the lack of interpretability of traditional deep learning models, it is difficult to gain clinical trust and medical guidelines and experts' experiences are not effectively incorporated, while purely symbolic systems are difficult to process visual data. NeuroSymAD[8] proposes to mimic the multi-modal diagnostic process of doctors through a neurosymbolic framework that combines deep learning (to process MRIs) and symbolic inference (to integrate clinical rules) while automatically generating medical rules with LLM. medical rules to improve diagnostic accuracy and interpretability.

However, whether using unimodal approaches or multi-modal integration with clinical data, these methods essentially stem from data-driven learning without modeling the causal structure in Alzheimer's disease (AD) diagnosis. Consequently, such non-causal models are vulnerable to interference from confounders. To address this, we use a Structural Causal Model (SCM) to guide AD diagnostic reasoning for multimodal data sources. Specifically, SCMs implement causal interventions by modeling the causal relationship between input data and diagnostic outcomes, which can effectively mitigate the effects of irrelevant confounders.

Therefore, we propose ADPC for AD diagnostics, a novel framework which integrates structural causal models to explicitly model the causal relationships between visual/textual features, confounders and diagnostic outcomes. Before training, we use Large Language Model (LLM) to generate the structured summaries through specific well-designed templates for filtering irrelevant text semantic information. These summaries, combined with MRI/fMRI images, serve as textual and visual inputs to the model. The visual inputs are fed into a pre-trained SwinUNETR feature extractor and a Visual Encoder to extract visual features. Textual inputs are processed through a SimpleTokenizer and a Textual Encoder to obtain textual features. Subsequently, the extracted visual and textual features are passed into the cross-modal Causal Fusion (CF) module to obtain an appropriate mediator. Meanwhile, the visual and textual features are concatenated to form multi-modal features. Ultimately, these multi-modal features are fed into a Multi-modal Encoder, a Front Door Adjustment module, and a classifier to produce the final outcome.

Overall, the main contributions of this paper are as follows:

- We implement LLM-guided clinical data summarization to enrich textual feature inputs. Utilizing specific prompts, large language model (LLM) transform unstructured clinical data into structured summarization. This approach aligns with knowledge distillation techniques, where LLM act as "teacher models" to generate high-fidelity representations of clinical

histories, medication records and behavioral symptoms, etc.

- We propose a causal intervention-based AD diagnostic framework to mitigate confounders' impact on diagnosis, achieving significant performance improvements.
- For the first time, we introduce a mediator generation module leveraging cross-modal fusion, which enables unified front-door adjustment on multi-modal features. This approach improves the accuracy of AD diagnosis.

## 2 Related Work

### 2.1 AD Diagnosis With Deep Learning

With the advancement of deep learning, its application in assisting the diagnosis of Alzheimer's disease (AD) and early-stage mild cognitive impairment (MCI) has proliferated, yielding promising results. Due to the subtle structural changes in the brain of early-stage patients, traditional methods rely on manual pre-selection of lesion regions and fail to integrate multi-modal clinical data (e.g., cognitive scores, genetic information), resulting in limited diagnostic accuracy. The authors propose to automatically learn lesion regions through hierarchical 3D fully convolutional networks and incorporate multi-modal feature fusion to improve the sensitivity and specificity of early diagnosis. Wang et al. proposed a hybrid-granularity ordinal prototype learning (HOPE)[21] method to predict MCI progression by integrating multi-granularity biomarkers and sequential cognitive features. Xue et al. demonstrated robust performance in classifying dementia etiologies using extensive multi-modal brain imaging data, leveraging spatial-temporal fusion techniques to capture dynamic functional connectivity patterns in structural MRI (sMRI). Notably, a neuro-symbolic framework, called NeuroSymAD, which is introduced to combine the neural networks with symbolic logic reasoning, enhancing both diagnostic accuracy and explainability. However, these methods fail to account for inherent data biases and confounding influences between inputs and diagnostic outcomes, as they operate under non-causal model. In contrast, our approach establishes a causal framework between inputs and outputs that explicitly identifies and mitigates confounding factors, thereby ensuring robust diagnostic reliability.

### 2.2 Causal Inference

The presence of confounders often lead to spurious correlations between inputs and outputs[3][12], resulting in abnormal model predictions. However, as confounders are inherently unobservable or statistically intractable, causal inference methodologies, including backdoor adjustment, front-door adjustment, and counterfactual intervention, which have become critical tools to mitigate these biases. These approaches demonstrate transformative potential across deep learning domains. For instance, Wang et al.[22] enhanced Fast R-CNN's performance by implementing backdoor adjustment to disentangle confounding visual features like lighting variations and background clutter. Liu et al.[10] proposed a novel framework CMCIR to discover cross-modal causal structures via causal intervention and achieved remarkable performance in

event-level visual question answering task. Chen et al.[2] sequentially applied front-door adjustments to visual representations and linguistic representations, significantly eliminating visual and linguistic confounders. Another breakthrough comes from Causal-Aware Attention Mechanism (CaaM)[23], which integrates causal intervention into attention mechanisms by reweighting attention scores using latent mediator variables, achieving a 23% accuracy improvement on out-of-distribution (OOD) data compared to standard self-attention.

These advancements demonstrate the potential of combining causal theory with deep learning and show great research value in improving the performance of deep learning in various domain applications through causal interventions such as front-door adjustment, back-door adjustment, and counterfactual interventions.

### 3 Method

In this section, we first present the overall framework of ADPC. Then We elaborate on how causal intervention eliminates visual and linguistic confounders through structural causal modeling (SCM). Finally, we demonstrate the application of well-designed prompts to guide large language model (LLM) in summarizing volunteers' clinical data.

#### 3.1 Framework

The core framework of ADPC is shown in Fig. 1. Our framework comprises six core components: a visual modality encoder, a textual modality encoder, a cross-modal Causal Fusion module (CF), a intervention module, a multi-modal feature encoder, and a classifier. Inspired by Xue et al.[24], we first perform self-supervised training on a SwinUNETR network[16]. Then we take out its encoder and freeze the weight as a feature extractor for multi-modal brain scans. Simultaneously, we employ structured prompt templates to guide DeepSeek[6] in generating comprehensive summaries from clinical data. To further enhance the representation quality of 3D brain scans, we utilize a Vision Transformer (ViT) with image patch embedding. For textual, we employ a feature extraction framework consisting of a SimpleTokenizer and a standard Transformer[19] encoder to extract the textual feature. Visual and textual features are first fed into the CF module to obtain the mediator  $M$  that contains information on casual inference. These two modality features are then concatenated and fed into the multi-modal encoder to obtain fused representations. Subsequently, the multi-modal features and mediator  $M$  undergo front-door intervention through Structural Causal Modeling (SCM) to eliminate confounding factors. Finally, the purified features are passed through the classification head to yield the prediction results.

#### 3.2 Causal Intervention

To formalize the causal intervention mechanism in our methodology, we adopt Judea Pearl's Structural Causal Model (SCM) framework, which is illustrated in Fig.2. The SCM provides a mathematical formalism for encoding causal relationships between variables through directed acyclic graphs (DAGs), where nodes represent observable variables and directed edges denote causal dependencies.

In Fig.2a, the causal effects of input variable  $X$  on output variable  $Y$  is formally represented as a directed edge  $X \rightarrow Y$  in the structural causal model (SCM).

This causal dependency is mathematically expressed through the conditional probability  $P(Y|X)$ , which quantifies the probabilistic influence of  $X$  on  $Y$  under observational conditions. However, the presence of biased data introduces the confounders  $S$ , which induce spurious correlations between input  $X$  and output  $Y$ . These confounding factors create non-causal dependencies that mislead model predictions, leading to systematic errors in decision-making. Consequently, in the presence of confounders, the true causal effects  $X \rightarrow Y$  cannot be reliably calculated through conditional probability alone. For instance, when diagnosing Alzheimer's disease (AD) based on hippocampal atrophy size observed in brain scans, age may act as a confounder that compromises diagnostic accuracy. This occurs because age-related mild hippocampal atrophy in elderly patients—particularly in the absence of supporting biomarkers could be misattributed to early AD pathological changes. Similarly, when diagnosing AD through neurological assessment in clinical data, age may function as a confounder. Artifacts in brain scan images may act as confounding factors in AD diagnosis, obscuring the true causal effects between visual features and diagnosis.

An effective method for mitigating confounders is through back-door adjustment. Back-door adjustment employs the do-calculus  $do(\cdot)$  to block the backdoor path  $Y \leftarrow S \rightarrow X$ , and its causal intervention process can be mathematically formalized as follows:

$$P(Y | do(X)) = \sum_s P(Y | X, S = s)P(S = s). \quad (1)$$

The aforementioned back-door adjustment formula can be interpreted as follows: For each known confounder  $S$ , the causal effect of  $X$  on  $Y$  is calculated by computing the weighted average of the effect estimates using the original distribution of  $S$  as the weighting factor.

Since back-door adjustment requires confounders to be observable and measurable, a condition rarely met due to the prevalence of latent confounders. Instead, we employ front-door adjustment to address unobserved confounders, as illustrated in Fig.2b. Front-door adjustment introduces a mediator  $M$  to eliminate the influence of unmeasurable confounders  $S$ , where  $M$  blocks the causal pathway  $S \rightarrow X \rightarrow M \rightarrow Y$  while satisfying the front-door criterion. The front-door criterion requires the following conditions: (1) $M$  intercepts all directed paths from  $X$  to  $Y$ . (2)There exists no unblocked backdoor path between  $X$  and  $M$ . (3)All backdoor paths from  $M$  to  $Y$  are blocked by conditioning on  $X$ . The causal effect under front-door adjustment can be mathematically formalized as:

$$\begin{aligned} P(Y | do(x)) &= \sum_m P(Y | do(M = m))P(M = m | X = x) \\ &= \sum_m P(M = m | X = x) \sum_{x'} P(Y | X = x', M = m)P(X = x'). \end{aligned} \quad (2)$$

The aforementioned front-door adjustment formula can be interpreted as follows:  $x'$  represents the natural value of variable  $X$  under no intervention, while  $\sum_{x'} P(Y | X = x', M = m)P(X = x')$  computes the causal effect of  $m$  on  $Y$  under the natural distribution of  $X$ , given  $M = m$ . Since there is no confounder between  $M$  and  $X$ , the formula calculates the conditional probability  $P(m | X)$

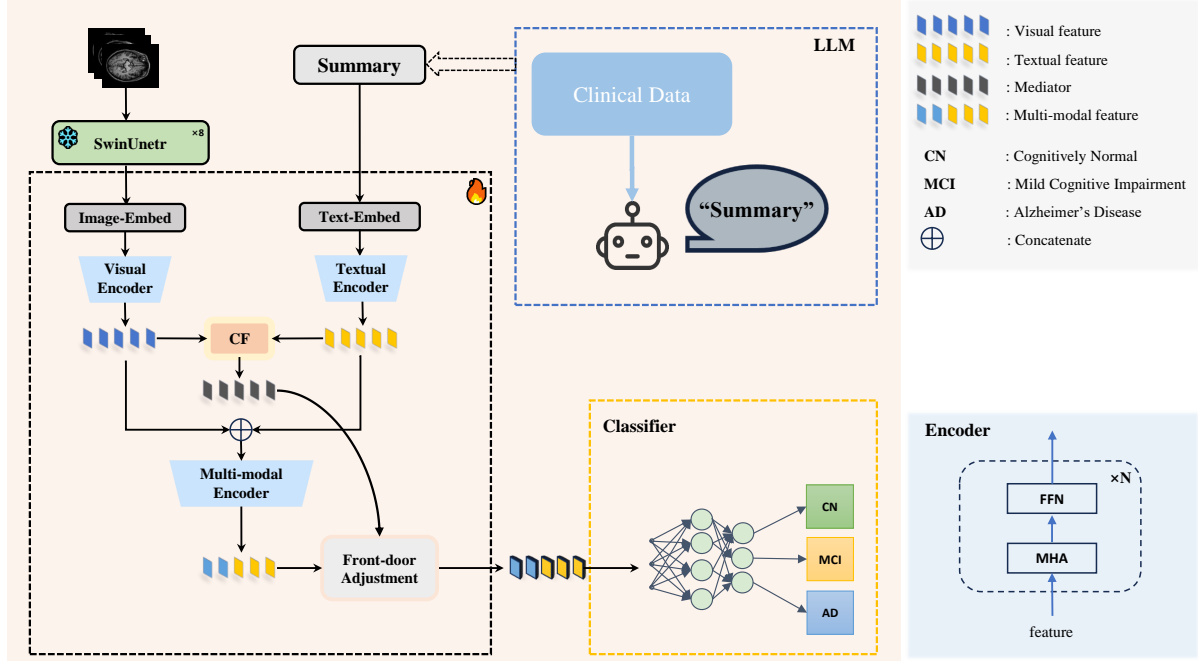


**Figure 1: An overview of our proposed ADPC.** MRI/fMRI scans and summary generated by large language model (LLM) are fed into the model. SwinUNETR [7] is used to extract visual features. Within the ADPC framework, visual and textual features are processed through the Cross-modal Causal Fusion (CF) module to generate mediator which subsequently undergo front-door adjustment to align with multi-modal features. Ultimately, features refined through front-door adjustment are fed into the classifier to generate final predictions.

and weights it by the causal effect of  $m$  on  $Y$ , yielding the total causal effect of  $X$  on  $Y$  through weighted averaging. As illustrated in Fig.2c, we construct the structural causal model (SCM) of the ADPC framework, where visual features  $V$  and textual features  $T$  generate causal effects on multi-modal features  $F$  and classification outcome  $R$  through forward propagation. However, the presence of unobserved confounders  $S$  induces spurious correlations between inputs  $V, T$  and outcome  $R$ . To address this, we implement front-door adjustment by introducing a mediator  $M$  to block the confounding path  $S \rightarrow V \rightarrow F \rightarrow M$  and  $S \rightarrow T \rightarrow F \rightarrow M$ , thereby isolating the true causal effects between multi-modal features and classification outcomes.

Specifically, we employ the cross-modal Causal Fuse (CF) module to estimate the mediator  $M$ , followed by an enhanced Front-door Adjustment (FDA) module to perform front-door adjustment on multi-modal features.

### 3.3 Cross-modal Causal Fusion Module

To obtain an optimal mediator  $M$ , we introduce the Cross-modal Causal Fusion (CF) Module, whose architecture is illustrated in Fig.3. The CF module operates through two key computational phases:

**3.3.1 Cross-modal Attention Computation.** Visual features (Textual features) serve as queries and Textual features (Visual features)

serve as keys and values in the multi-head attention (MHA) mechanism respectively for generating features  $f_{VTT}$  and  $f_{TVV}$  through Multi-Head Attention.  $f_{VTT}$  and  $f_{TVV}$  are then concatenated to calculate cross-modal features  $f_{cm}$ :

$$f_{VTT} = \alpha \cdot MHA(Q_V, K_T, V_T), \quad (3)$$

$$f_{TVV} = \beta \cdot MHA(Q_T, K_V, V_V), \quad (4)$$

and

$$f_{cm} = f_{VTT} \oplus f_{TVV}. \quad (5)$$

Here,  $\alpha$  and  $\beta$  are trainable parameters of the model. MHA is Multi-Head Attention Layer.  $\oplus$  denotes concatenation.

**3.3.2 Causal Attention Computation.** The cross-modal features obtained from the previous step are then fed into the Causal Attention Module (CaaM) [23] block, which implements a dual-phase confounding suppression mechanism to derive the final mediator  $M$ :

$$M = LN(CaaM(f_{cm})), \quad (6)$$

where  $M$  denotes Mediator and  $LN$  is layer normalization.

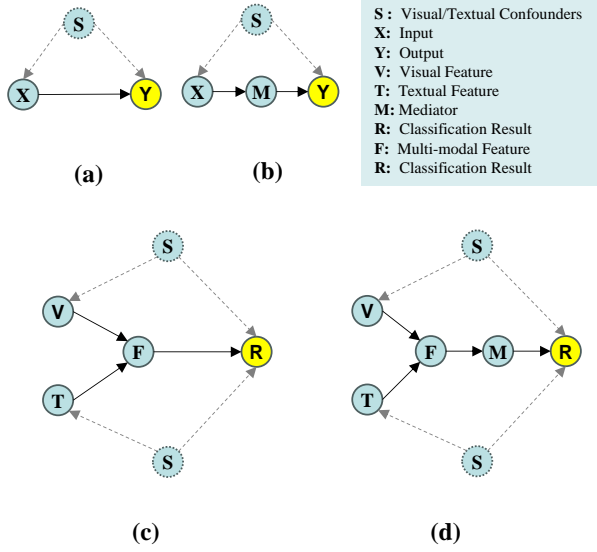


Figure 2: The structural causal model (SCM). (a) illustrates the causal pathway from input  $X$  to output  $Y$ , where both  $X$  and  $Y$  are influenced by the confounding factor  $S$ . (b) demonstrates the application of front-door adjustment to decompose the causal pathway from  $X$  to  $Y$  and estimate the causal effect between them when confounders are unobservable. (c) illustrates the structural causal model (SCM) diagram constructed based on our proposed framework. (d) demonstrates the implementation of front-door adjustment in our framework to address unobservable visual and textual confounders by selecting appropriate mediators for multi-modal features.

### 3.4 Front-door Adjustment

To calculate the true causal effects between multi-modal feature  $F$  and classification outcomes  $R$ , we first calculate  $F$  as follows:

$$F = fv \oplus ft. \quad (7)$$

Inspired by [2] for applying front-door adjustment to deep learning frameworks, we implement a similar approach in the ADPC model to estimate Eq.2. The workflow of front-door adjustment in ADPC is as follows:

#### 1. $P(R | do(m))$ Estimation

$$\begin{aligned} P(R | do(m)) &= \sum_{f'} P(Y | F = f', M = m) P(F = f') \\ &\approx \text{softmax}\left(\frac{FM^T}{\sqrt{d_k}}\right) F \\ &= M_{do}, \end{aligned} \quad (8)$$

where  $F$  and  $R$  denote multi-modal features and classification result.  $fv$  and  $ft$  are visual features and textual features.  $do(M)$ , which helps the model learn the true causal effects between  $F$  and  $R$ , denotes an intervention on  $M$ .  $M_{do}$  represents the true causal effects

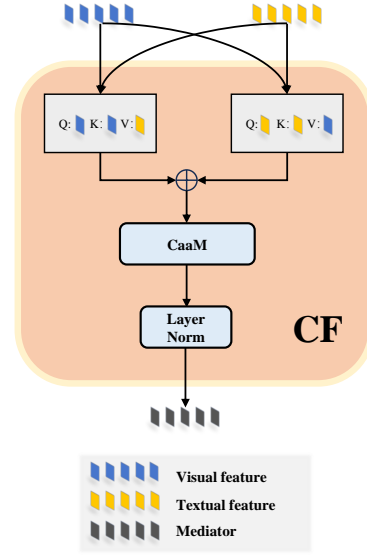


Figure 3: The structure of Cross-modal Causal Fusion (CF) module. Visual feature and textual feature undergo cross-attention computation and are concatenated. The fused features are then passed through the CaaM [23] to further eliminate confounders, ultimately outputting the refined representation as the mediator.

$M \rightarrow R$ .

#### 2. $P(R | do(F))$ Estimation

$$\begin{aligned} P(R | do(F)) &= \sum_m P(M = m | F = f) P(R | do(M = m)) \\ &= \sum_m P(M = m | F = f) \sum_{f'} P(Y | F = f', M = m) P(F = f'), \\ &\approx \text{softmax}\left(\frac{FM^T}{\sqrt{d_k}}\right) M \end{aligned} \quad (9)$$

where  $M$  denotes Mediator and  $do(\cdot)$  is a central tool in causal inference for modelling active interventions in variables.

### 3.5 Textual Data Generation

In the collected medical datasets, we first systematically remove diagnostic data containing identifiable patterns to prevent outcome bias. This process ensures the reliability of the analysis. To enhance the acquisition of volunteer textual information for the ADPC, we then leverage the Large Language Model to integrate and summarize preprocessed clinical data, ultimately generating tokenized outputs. The subsequent phase employs a structured prompt template and a standardized volunteer information summarization framework to maximize the comprehensiveness of AI-generated outputs. In Figure 5, this template systematically captures critical

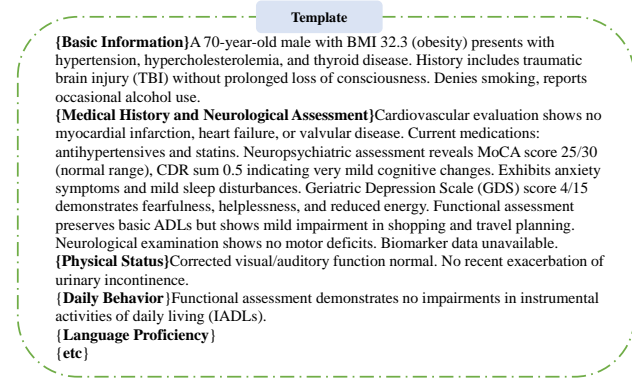


**Figure 4: An example of summary generated by LLM through a structured prompt template, which contains the core information of a CN volunteer.**

dimensions of volunteer profiles through the following aspects: **Basic Information, Medical History and Neurological Assessment, Physical status, Daily Behavior, language proficiency, etc.** When encountering unrecorded medical data, we configure large language model (LLM) to skip processing these cases.

### 3.6 Pseudo Code

We summarize the pseudo code of the proposed ADPC as follow:

---

**Algorithm 1** Training procedure of ADPC.

---

**Input:** MRI / fMRI data  $v \in \mathbb{R}^{h \times w \times d}$ , clinical summary  $t$ , labels  $l$

**Output:** Parameters  $\theta$  of ADPC

```

1: for batch  $(v, t, l)$  in loader do
2:    $v' \leftarrow \text{SwinUNETR\_Encoder}(v)$ 
3:    $f_v \leftarrow \text{Visual\_Encoder}(v')$ 
4:    $f_t \leftarrow \text{Textual\_Encoder}(t)$ 
5:   Mediator  $\leftarrow \text{CF}(f_v, f_t)$  //Cross-modal Causal Fusion
6:    $f_{mm} \leftarrow \text{Multi-modal\_Encoder}(\text{concat}(f_v, f_t))$ 
7:    $f_{out} \leftarrow \text{FDA}(f_{mm}, \text{Mediator})$  //Front-door Adjustment
8:    $y_p \leftarrow \text{Classifier}(f_{out})$ 
9:    $\mathcal{L} \leftarrow \text{CE}_{Loss}(y_p, l)$ 
10:  update model  $\theta$  to minimize  $\mathcal{L}$ 
11: end for
```

---

## 4 Experiment

### 4.1 Datasets

Our experiment used two Alzheimer’s disease (AD) research databases: the National Alzheimer’s Coordinating Center (NACC)[1] and Alzheimer’s Disease Neuroimaging Initiative (ADNI)[14] datasets. Both repositories provide multi-modal neuroimaging, clinical, and biomarker data essential for investigating AD progression mechanisms. ADNI synthesizes multi-modal data from 63 research centers globally to elucidate AD pathological mechanisms and identify early diagnostic biomarkers. NACC consolidates multi-center clinical-pathological data across 39 U.S. Alzheimer’s Disease Research Centers (ADRCs),

providing robust infrastructure for dementia research. The ADNI dataset has approximately 20%-30% of total participants for CN and 40%-50% for MCI, the focus populations of the ADNI study, and approximately 20%-30% for AD. The total number of participants in the NACC is over 51,269. The total number of participants in CN, MCI and AD are about 33.6%, 14.8% and 31.5% respectively.

The experiment used neuroimaging and clinical data from 2,388 participants in the NACC dataset and participants subjects in the ADNI dataset and they are divided into 8:1:1, respectively, with 80% as the training set, 10% as the validation set, and 10% as the test set. Each volunteer we selected had a MRI scan as well as a clinical data correspondence. Table 2 shows the basic information of NACC dataset and ADNI dataset.

We conducted independent training, validation and testing procedures for the ADNI and NACC datasets to ensure rigorous evaluation of model generalizability. The total number of samples used to train our model with the ADNI dataset is smaller than HOPE[21] and NeuroSysAD[8].

### 4.2 Experimental Settings

We selected MRI scans from the NACC dataset and ADNI as visual inputs. All MRI scans acquired from participants underwent preprocessing steps, including spatial resampling, intensity normalization, and automated foreground extraction. All volumetric data were uniformly resized to  $128 \times 128 \times 128$ .

Clinical data were fed into DeepSeek[6] to generate summary. The template shown in Fig. 4 was utilized to constrain the structure of the LLM’s text output.

We performed the CN/MCI/AD triple classification task on both the ADNI and the NACC datasets, and the CN/AD binary classification task on the NACC dataset. Five evaluation metrics were used in our task: classification accuracy (ACC), area under the receiver operating characteristic curve (AUC), F1-score, Recall and Precision.

### 4.3 Implementation Details

The SwinUNETR feature extractor was optimized using an AdamW optimizer [11]. We set the initial learning rate to  $4e-4$  with cosine annealing scheduling (warmup ratio=0.1). The weight decay rate of AdamW was set to 0.1 and the batch size was set to 2. The training protocol implemented on an NVIDIA L20 GPU platform.

The ADPC model was trained on an NVIDIA H20 GPU platform using the same optimization framework as SwinUNETR, which included the AdamW optimizer and a cosine annealing learning rate scheduler with a 0.001 warmup phase. To adapt to architectural requirements and improve training dynamics, the initial learning rate was set to  $5e-4$ . The batch size was set to 16. Both the Visual Encoder and Textual Encoder contain 6 standard transformer[19] encoder blocks, while the Multi-modal Encoder contains 4 standard transformer encoder blocks.

### 4.4 Performance Comparison

As quantitatively demonstrated in Table 1, the proposed ADPC framework achieved superior performance in three-class classification and two-class classification tasks across both NACC and ADNI datasets.



**Table 1: Performance of various methods in CN/MCI/AD classification. The best results are highlighted in bold.**

Dataset Metrics Method	NACC					ADNI				
	ACC (%)	F1 (%)	Precision (%)	Recall (%)	AUC (%)	ACC (%)	F1 (%)	Precision (%)	Recall (%)	AUC (%)
ViT [4]	43.6	43.5	45.1	43.7	64.1	58.1	58.0	58.5	57.4	59.3
3D-ResNet <sub>3</sub> [9]	58.1	58.0	58.5	57.4	59.3	65.0	66.2	67.6	64.7	66.2
OR-CNN [13]	61.7	60.8	60.7	60.8	61.4	65.7	66.9	69.0	64.9	66.9
ADRank [15]	63.4	62.1	63.0	60.9	63.0	67.0	67.9	68.4	65.7	67.9
CORF [26]	64.1	62.8	63.2	62.1	63.5	67.8	68.1	69.0	67.2	68.1
HOPE [21]	67.6	66.4	66.1	67.2	66.8	72.0	71.1	71.3	71.0	71.3
<b>ADPC(ours)</b>	<b>75.7</b>	<b>74.4</b>	<b>75.3</b>	<b>73.5</b>	<b>88.9</b>	<b>80.7</b>	<b>78.7</b>	<b>79.4</b>	<b>78.0</b>	<b>93.5</b>

**Table 2: Basic information of the dataset used in the experiment.**

Method Dataset	ADPC(ours)			HOPE[21]			NeuroSysAD[8]		
	Group	Count	(%)	Group	Count	(%)	Group	Count	(%)
ADNI	NC	351	50.2%	NC	317	30.2%	NC	-	-
	MCI	185	26.5%	MCI	486	46.3%	MCI	-	-
	AD	163	23.3%	AD	247	23.5%	AD	-	-
	ALL	699	100.0%	ALL	1050	100.0%	ALL	3088	100.0%
NACC	NC	900	37.5%	NC	-	-	NC	-	-
	MCI	909	38.0%	MCI	-	-	MCI	-	-
	AD	589	24.5%	AD	-	-	AD	-	-
	ALL	2398	100%	ALL	-	-	ALL	-	-

For the three-class classification experiments, we utilized the classification results from HOPE as the comparative benchmark and we utilized the classification results from NeuroSysAD for the binary classification experiments.

In detail, our ADPC method achieves better performance compared to prior works [21], [13], [9], [15], [26], [4] on the ADNI dataset despite utilizing a smaller training cohort, achieving improvements of 8.1%, 4%, 5%, 6% and 22.1% of ACC, F1-score, Precision, Recall and AUC for AD/MCI/CN classification. Compared to the performance of prior works on external NACC testing set, our ADPC method also achieves better performance when trained and tested on NACC dataset.

As exemplified in Table 3, within the ADNI test cohort, the ADPC framework demonstrates superior capability in distinguishing AD from CN. Compared to the best result of prior works [5], [17], [20], [8], ADPC achieves improvements of 4.4%, 4.6% and 2.6% of ACC, AUC and Precision.

#### 4.5 Ablation Study

To quantitatively assess the efficacy of the proposed front-door adjustment and cross-modal Causal Fusion(CF) module, we conducted controlled ablation experiments by systematically removing both the CF module and the front-door adjustment stage. As demonstrated in Table 4, the experimental results in the NACC test cohort revealed statistically significant performance degradation in all metrics, with the classification ACC decreasing 2.7%, AUC scores decreasing 0.5%, the F1-score decreasing 2.6%, the precision decreasing 3.5% and the recall decreasing 0.5%. These findings conclusively

validate the critical role of the CF module and front-door adjustment in improving the model's performance. This demonstrates that incorporating appropriate front-door adjustments in classification models effectively mitigates the influence of confounders, thereby enhancing diagnostic accuracy.

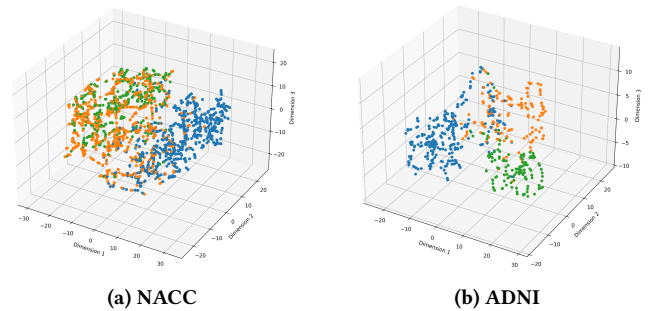


**Figure 5: Visualization of feature distribution within our proposed ADPC. (a) Visualization on NACC dataset. (b) Visualization on ADNI dataset.**

#### 4.6 Visualization

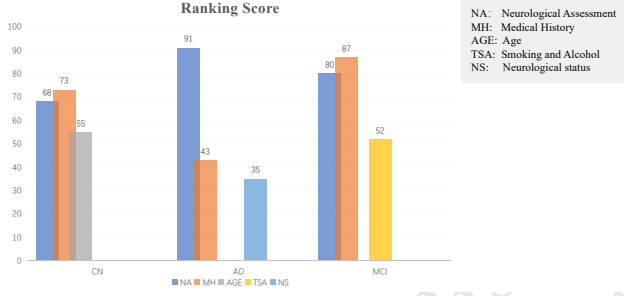
To geometrically characterize the framework's class discriminability, we performed nonlinear dimensionality reduction using t-distributed stochastic neighbor embedding (t-SNE)[18], projecting high-dimensional feature representations from both NACC and ADNI datasets into

**Table 3: Performance of various methods in CN/AD classification. The best results are highlighted in bold.**

Dataset Metrics Method	ADNI				
	ACC (%)	F1 (%)	Precision (%)	Recall (%)	AUC (%)
Opt 3D CNN [17][8]	81.6	85.9	80.2	92.42	89.2
DA CNN [20]	86.4 [8]	88.5	86.9	93.24	89.2
3D-ResNet <sub>2</sub> [5] [8]	85.7	90.46	86.16	<b>95.2</b>	93.4
NeuroSysAD [8]	88.6	<b>92.2</b>	89.9	94.4	92.6
<b>ADPC(ours)</b>	<b>92.2</b>	90.9	<b>92.5</b>	89.4	<b>96.9</b>

**Table 4: Ablation performance with and without cross-modal Causal Fusion(CF) module and Front-door Adjustment(FDA) on NACC dataset.**

Dataset Metrics Method	NACC				
	ACC (%)	F1 (%)	Precision (%)	Recall (%)	AUC (%)
ADPC(ours)	<b>75.7</b>	<b>74.4</b>	<b>75.3</b>	<b>73.5</b>	<b>88.9</b>
- CF & FDA	72.2	70.8	71.6	70.2	87.8

**Figure 6: Visualization of Ranking Scores. The Ranking Scores highlight the top three elements that the model focuses attention on, within the summary generated by LLM.**

three-dimensional latent spaces. As visualized in Fig.5, we use different colors to indicate the true labels of the data points. There is a good degree of segmentation between different categories of data points.

Furthermore, we conducted gradient saliency analysis on the text embedding layer to quantify lexical sensitivity toward target categories. Specifically, we computed gradient tensors of embedding weights through backpropagation, which enables efficient per-embedding gradient norm calculation without full gradient instantiation. This process yields a  $\nabla_{\mathbf{w}} \in \mathbb{R}^{v \times d}$  matrix where each row vector represents the sensitivity magnitude of corresponding vocabulary item ( $v$ =vocab size,  $d$ =embedding dimension). As visualized in Fig.6, we sampled 25 instances and evaluated the top five sensitivity-ranked features through scoring for each category. By decoding the corresponding word vectors into words, we successfully identified the three primary objects of attention that the model prioritized during processing.

Fig.6 revealed that the model exhibited significantly heightened attention to neurological assessment results in AD volunteers, with scores substantially surpassing other evaluation metrics. In contrast, for CN and MCI volunteers, the model primarily focused on medical history documentation.

The score also further revealed that age serves as a critical determinant in distinguishing cognitively normal (CN) individuals, while smoking and alcohol consumption emerged as pivotal indicators for identifying Mild Cognitive Impairment (MCI), aligning with the research on modifiable risk factors in cognitive aging.

During the visualization process, we observed that our ADPC model specifically focuses on the term "female" when diagnosing female volunteers with Alzheimer's disease (AD), a phenomenon consistent with established research [25] indicating women's heightened susceptibility to AD development.

## 5 Conclusion

In this paper, we propose a Structural Causal Model to model the causal relationship between clinical input and Alzheimer's disease diagnosis. Based on this foundation, we propose ADPC, a framework for Alzheimer's diagnosis through multi-modal information. We implement causal intervention to eliminate to eliminate confounders that may lead to misdiagnosis. Specifically, ADPC enhances diagnostic confidence via our cross-modal Causal Fusion module and front-door adjustment. Pre-trained on the NACC and ADNI datasets, our method demonstrates competitive performance compared to other methods.

## References

- [1] Duane L Beekly, Erin M Ramos, Gerald van Belle, Woodrow Deitrich, Amber D Clark, Mary E Jacka, Walter A Kukull, et al. 2004. The national Alzheimer's coordinating center (NACC) database: an Alzheimer disease database. *Alzheimer Disease & Associated Disorders* 18, 4 (2004), 270–277.
- [2] Weixing Chen, Yang Liu, Ce Wang, Jiarui Zhu, Shen Zhao, Guanbin Li, Cheng-Lin Liu, and Liang Lin. 2023. Cross-modal causal intervention for medical report generation. *arXiv preprint arXiv:2303.09117* (2023).



- [3] Shachi Deshpande, Zheng Li, and Volodymyr Kuleshov. 2022. Multi-Modal Causal Inference with Deep Structural Equation Models. *arXiv preprint arXiv:2203.09672* (2022).
- [4] Alexey Dosovitskiy, Lucas Beyer, Alexander Kolesnikov, Dirk Weissenborn, Xi-aohua Zhai, Thomas Unterthiner, Mostafa Dehghani, Matthias Minderer, Georg Heigold, Sylvain Gelly, et al. 2020. An image is worth 16x16 words: Transformers for image recognition at scale. *arXiv preprint arXiv:2010.11929* (2020).
- [5] Amir Ebrahimi, Suhui Luo, and Raymond Chiong. 2020. Introducing transfer learning to 3D ResNet-18 for Alzheimer's disease detection on MRI images. In *2020 35th international conference on image and vision computing New Zealand (IVCNZ)*. IEEE, 1–6.
- [6] Daya Guo, Dejian Yang, Haowei Zhang, Junxiao Song, Ruoyu Zhang, Runxin Xu, Qihao Zhu, Shirong Ma, Peiyi Wang, Xiao Bi, et al. 2025. Deepseek-r1: Incentivizing reasoning capability in llms via reinforcement learning. *arXiv preprint arXiv:2501.12948* (2025).
- [7] Ali Hatamizadeh, Vishwesh Nath, Yucheng Tang, Dong Yang, Holger R Roth, and Daguang Xu. 2021. Swin unetr: Swin transformers for semantic segmentation of brain tumors in mri images. In *International MICCAI brainlesion workshop*. Springer, 272–284.
- [8] Yexiao He, Ziyao Wang, Yuning Zhang, Tingting Dan, Tianlong Chen, Guorong Wu, and Ang Li. 2025. NeuroSymAD: A Neuro-Symbolic Framework for Interpretable Alzheimer's Disease Diagnosis. *arXiv preprint arXiv:2503.00510* (2025).
- [9] Sergey Korolev, Amir Safiullin, Mikhail Belyaev, and Yulia Dodonova. 2017. Residual and plain convolutional neural networks for 3D brain MRI classification. In *2017 IEEE 14th international symposium on biomedical imaging (ISBI 2017)*. IEEE, 835–838.
- [10] Yang Liu, Guanbin Li, and Liang Lin. 2023. Cross-modal causal relational reasoning for event-level visual question answering. *IEEE Transactions on Pattern Analysis and Machine Intelligence* 45, 10 (2023), 11624–11641.
- [11] Ilya Loshchilov and Frank Hutter. 2017. Decoupled weight decay regularization. *arXiv preprint arXiv:1711.05101* (2017).
- [12] Xuan Ma, Xiaoshan Yang, and Changsheng Xu. 2023. Multi-source knowledge reasoning graph network for multi-modal commonsense inference. *ACM Transactions on Multimedia Computing, Communications and Applications* 19, 4 (2023), 1–17.
- [13] Zhenxing Niu, Mo Zhou, Le Wang, Xinbo Gao, and Gang Hua. 2016. Ordinal regression with multiple output cnn for age estimation. In *Proceedings of the IEEE conference on computer vision and pattern recognition*. 4920–4928.
- [14] Ronald Carl Petersen, Paul S Aisen, Laurel A Beckett, Michael C Donohue, Anthony Collins Gamst, Danielle J Harvey, CR Jack Jr, William J Jagust, Leslie M Shaw, Arthur W Toga, et al. 2010. Alzheimer's disease Neuroimaging Initiative (ADNI) clinical characterization. *Neurology* 74, 3 (2010), 201–209.
- [15] Hezhe Qiao, Lin Chen, and Fan Zhu. 2022. Ranking convolutional neural network for Alzheimer's disease mini-mental state examination prediction at multiple time-points. *Computer Methods and Programs in Biomedicine* 213 (2022), 106503.
- [16] Yucheng Tang, Dong Yang, Wenqi Li, Holger R Roth, Bennett Landman, Daguang Xu, Vishwesh Nath, and Ali Hatamizadeh. 2022. Self-supervised pre-training of swin transformers for 3d medical image analysis. In *Proceedings of the IEEE/CVF conference on computer vision and pattern recognition*. 20730–20740.
- [17] Rosanna Turrise, Alessandro Verri, and Annalisa Barla. 2023. The effect of data augmentation and 3D-CNN depth on Alzheimer's Disease detection. *arXiv preprint arXiv:2309.07192* (2023).
- [18] Laurens Van der Maaten and Geoffrey Hinton. 2008. Visualizing data using t-SNE. *Journal of machine learning research* 9, 11 (2008).
- [19] Ashish Vaswani, Noam Shazeer, Niki Parmar, Jakob Uszkoreit, Llion Jones, Aidan N Gomez, Łukasz Kaiser, and Illia Polosukhin. 2017. Attention is all you need. *Advances in neural information processing systems* 30 (2017).
- [20] Shravan Venkatraman et al. 2024. A Dual-Attention Aware Deep Convolutional Neural Network for Early Alzheimer's Detection. *arXiv e-prints* (2024), arXiv–2407.
- [21] Chenhui Wang, Yiming Lei, Tao Chen, Junping Zhang, Yuxin Li, and Hongming Shan. 2024. Hope: Hybrid-granularity ordinal prototype learning for progression prediction of mild cognitive impairment. *IEEE Journal of Biomedical and Health Informatics* 28, 11 (2024), 6429–6440.
- [22] Tan Wang, Jianqiang Huang, Hanwang Zhang, and Qianru Sun. 2020. Visual commonsense representation learning via causal inference. In *Proceedings of the IEEE/CVF Conference on Computer Vision and Pattern Recognition Workshops*. 378–379.
- [23] Tan Wang, Chang Zhou, Qianru Sun, and Hanwang Zhang. 2021. Causal attention for unbiased visual recognition. In *Proceedings of the IEEE/CVF international conference on computer vision*. 3091–3100.
- [24] Chonghua Xue, Sahana S Kowshik, Dalia Lteif, Shreyas Puducheri, Varuna H Jasodanand, Olivia T Zhou, Anika S Walia, Osman B Guney, J Diana Zhang, Serena T Pham, et al. 2024. AI-based differential diagnosis of dementia etiologies on multimodal data. *Nature Medicine* 30, 10 (2024), 2977–2989.
- [25] Yan Yan, Xinming Wang, Dale Chaput, Min-Kyoo Shin, Yeojung Koh, Li Gan, Andrew A Pieper, Jung-AA Woo, and David E Kang. 2022. X-linked ubiquitin-specific peptidase 11 increases tauopathy vulnerability in women. *Cell* 185, 21 (2022), 3913–3930.
- [26] Haiping Zhu, Hongming Shan, Yuheng Zhang, Lingfu Che, Xiaoyang Xu, Junping Zhang, Jianbo Shi, and Fei-Yue Wang. 2021. Convolutional ordinal regression forest for image ordinal estimation. *IEEE transactions on neural networks and learning systems* 33, 8 (2021), 4084–4095.